



## Long-term trends in the atmospheric water vapor content estimated from ground-based GPS data

T. Nilsson<sup>1</sup> and G. Elgered<sup>1</sup>

Received 12 March 2008; revised 29 June 2008; accepted 16 July 2008; published 1 October 2008.

[1] We have used 10 years of ground-based data from the Global Positioning System (GPS) to estimate time series of the excess propagation path due to the gases in the neutral atmosphere. We first derive the excess path caused by water vapor which in turn is used to infer the water vapor content above each one of 33 GPS receiver sites in Finland and Sweden. Although a 10 year period is much too short to search for climate change we use the data set to assess the stability and consistency of the linear trend of the water vapor content that can be estimated from the data. The linear trends in the integrated water vapor content range from  $-0.2$  to  $+1.0$   $\text{kg m}^{-2} \text{decade}^{-1}$ . As one may expect we find different systematic patterns for summer and winter data. The formal uncertainty of these trends, taking the temporal correlation of the variability about the estimated model into account, are of the order of  $0.4$   $\text{kg m}^{-2} \text{decade}^{-1}$ . Mostly, this uncertainty is due to the natural short-term variability in the water vapor content, while the formal uncertainties in the GPS measurements have only a small impact on the trend errors.

**Citation:** Nilsson, T., and G. Elgered (2008), Long-term trends in the atmospheric water vapor content estimated from ground-based GPS data, *J. Geophys. Res.*, 113, D19101, doi:10.1029/2008JD010110.

### 1. Introduction

[2] Water vapor in the atmosphere is a parameter of great importance in climate models because of its role as a greenhouse gas. In fact water vapor is a very efficient greenhouse gas. An increase of 20% of the water vapor content in the tropics has a larger impact than a doubling of the carbon dioxide concentration [Buehler *et al.*, 2006]. In this presentation we will focus on the integrated water vapor (IWV).

[3] The direct human influence on the IWV is almost negligible [Intergovernmental Panel on Climate Change, 2007]. However, water vapor feedback is one of the most important climate feedback processes. An increase of temperature due to, e.g., emission of other greenhouse gases will result in an increase in IWV since the equilibrium vapor pressure increases with increasing temperature. Typically climate models tend to predict that the average relative humidity is conserved when the temperature changes [Trenberth *et al.*, 2003]. The relationship between changes in the IWV and changes in the temperature was recently assessed by Mears *et al.* [2007]. They found that an increase of the temperature of 1 K will result in an IWV increase by 5–7%. Using long time series of IWV and temperature this dependence can be tested. Furthermore, if the relative humidity is conserved, long time series of IWV measurements can be used as an independent data source to detect global warming. In all applications for monitoring of

climate change high long-term stability of the measurements is needed.

[4] A number of different studies to measure trends in IWV have been performed. Ross and Elliott [1996] studied the trends in IWV over North America as measured by radiosondes. Their analysis was later extended to the whole Northern Hemisphere [Ross and Elliott, 2001]. Overall they found an increase of IWV for the period 1973–1995, although there were large regional variations and even negative trends in some regions. However, extending this analysis to include periods after 1995 is problematic because of large changes in the radiosonde types at the end of 1995 and later [Elliott *et al.*, 2002; Trenberth *et al.*, 2005]. Bengtsson *et al.* [2004] studied temperature and IWV trends obtained from the ERA40 data set and found a global increase in IWV ( $+0.36$   $\text{kg m}^{-2} \text{decade}^{-1}$ ) which was twice as large as could be expected from the global temperature trend ( $+0.11$   $\text{K decade}^{-1}$ ). The likely reason for this was identified as an artifact caused by the changes in the global observing systems over the last decades. Similar conclusions were drawn by Trenberth *et al.* [2005] who compared trends obtained from ERA40, NCEP reanalysis, satellite measurements and the radiosonde data used by Ross and Elliott [2001].

[5] Global Navigation Satellite Systems (GNSS) can be used as a tool to estimate the IWV in the atmosphere. Most of the observations and studies on the accuracy of GNSS estimation of IWV carried out so far have used data from the Global Positioning System (GPS) [see, e.g., Tralli and Lichten, 1990; Bevis *et al.*, 1992; Emaradson *et al.*, 1998; Hagemann *et al.*, 2003; Gutman *et al.*, 2004]. Today there are many national and international GPS networks that have been operating for more than 10 years.

<sup>1</sup>Onsala Space Observatory, Department of Radio and Space Science, Chalmers University of Technology, Onsala, Sweden.

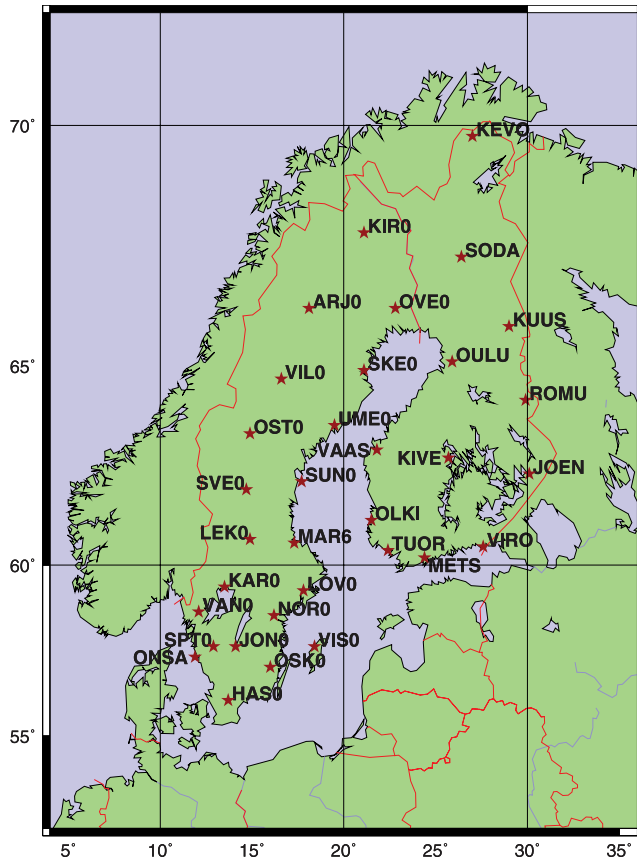


**Figure 1.** GPS receiver sites in the Swedish SWEPOS network and the Finnish FinnRef network.

[6] Relatively few investigations of trends estimated using GPS have been performed to date. *Gradinarsky et al.* [2002] investigated IWV trends over Sweden for the years 1993–2001, and found positive trends in general. *Jin et al.* [2007] used estimated trends in the Zenith Total Delay (ZTD) from a large number of globally distributed GPS sites, and found an average ZTD trend of  $15 \text{ mm decade}^{-1}$  (corresponding to an IWV trend of  $2 \text{ kg m}^{-2} \text{ decade}^{-1}$ , assuming that the average hydrostatic delay does not change). There were, however, large regional variations including large negative trends at some sites. A comparison of trends estimated by GPS and the similar technique VLBI (Very Long Baseline Interferometry) was done by *Steigenberger et al.* [2007]. They showed that the trends estimated using the two techniques only agree when ZTD estimates from both techniques are available simultaneously, demonstrating that the estimated trend is very sensitive to the time period used. The same conclusions were drawn by *Haas et al.* [2003].

[7] In this work we study the trends in IWV estimated using GPS data from Sweden and Finland acquired over a 10 year period. We begin in section 2 with a summary of the background theory. In section 3 we describe the analysis of GPS data. Thereafter, in section 4, the derivation of IWV from the estimated propagation delays is described together with examples of IWV time series. Sections 5 and 6 present the estimation of linear trends and their uncertainties,

respectively. The results are discussed in section 7, and section 8 ends the paper with the conclusions.

## 2. Theoretical Background

[8] The atmospheric parameter estimated in the GPS data processing is the equivalent excess propagation path referred to the zenith direction, often called the Zenith Total Delay (ZTD). It is often expressed in units of length, using the speed of light in vacuum for the conversion from a time delay. The ZTD,  $\ell_t$ , can be divided into a Zenith Hydrostatic Delay (ZHD),  $\ell_h$ , and a Zenith Wet Delay (ZWD),  $\ell_w$  [*Davis et al.*, 1985]:

$$\ell_t = \ell_h + \ell_w \quad (1)$$

[9] The hydrostatic term can be determined with an uncertainty of less than 1 mm in the zenith direction if the total ground pressure is measured with an uncertainty of less than 0.5 hPa [*Davis et al.*, 1985]. The ZWD can be written as [*Elgered*, 1993]:

$$\ell_w = 24 \cdot 10^{-6} \int_0^{\infty} \frac{e}{T} dh + 0.3754 \int_0^{\infty} \frac{e}{T^2} dh \quad [\text{m}] \quad (2)$$

where  $e$  is of the partial pressure of water vapor and  $T$  is the temperature, expressed in hPa and K, respectively. The expression for the IWV is similar:

$$V = \int_0^{\infty} \rho_v dh \quad (3)$$

where  $\rho_v$  is the absolute humidity in  $\text{kg m}^{-3}$ . The ZWD is related to the IWV because, according to the ideal gas law,  $\rho_v$  is proportional to  $e/T$ . A conversion factor  $Q$ :

$$Q = \frac{\ell_w}{V} \quad (4)$$

can be calculated by assuming a value of the mean temperature of the wet refractivity in the atmosphere. This conversion factor can be modeled, e.g., using a history of radiosonde data [*Emardson and Derks*, 2000], or calculated using reanalysis data from a numerical weather model such as the ECMWF model [*Wang et al.*, 2005]. These studies have shown that the IWV can be estimated from the ZWD with a typical root-mean-square (RMS) conversion error of less than 2%.

## 3. Analysis of GPS Data From SWEPOS and FinnRef

[10] We have used data from 33 GPS receiver sites in Sweden and Finland. The sites are of geodetic quality, meaning that they are mounted on solid bedrock. Most of the Swedish and Finnish sites have been in continuous operation since late 1993 and late 1996, respectively. Figure 1 shows the sites. Their names and coordinates are

**Table 1.** GPS Sites, Sorted by Decreasing Latitude

| Site    |            | Longitude (°E) | Latitude (°N) | Height <sup>a</sup> (m) |
|---------|------------|----------------|---------------|-------------------------|
| Acronym | Full Name  |                |               |                         |
| KEVO    | Kevo       | 27.007         | 69.756        | 111                     |
| KIRO    | Kiruna     | 21.060         | 67.877        | 469                     |
| SODA    | Sodankylä  | 26.389         | 67.421        | 279                     |
| ARJ0    | Arjeplog   | 18.125         | 66.318        | 459                     |
| OVE0    | Över Kalix | 22.770         | 66.310        | 200                     |
| KUUS    | Kuusamo    | 29.033         | 65.910        | 361                     |
| OULU    | Oulu       | 25.893         | 65.086        | 71                      |
| SKE0    | Skellefteå | 21.050         | 64.880        | 59                      |
| VIL0    | Vilhelmina | 16.559         | 64.697        | 420                     |
| ROMU    | Romuvaara  | 29.932         | 64.217        | 224                     |
| UME0    | Umeå       | 19.509         | 63.578        | 32                      |
| OST0    | Östersund  | 14.858         | 63.442        | 459                     |
| VAAS    | Vaasa      | 21.771         | 62.961        | 40                      |
| KIVE    | Kivetty    | 25.702         | 62.820        | 198                     |
| JOEN    | Joensuu    | 30.096         | 62.391        | 97                      |
| SUN0    | Sundsvall  | 17.659         | 62.232        | 7                       |
| SVE0    | Sveg       | 14.700         | 62.017        | 458                     |
| OLKI    | Olkiluoto  | 21.473         | 61.240        | 12                      |
| LEK0    | Leksand    | 14.877         | 60.722        | 448                     |
| MAR6    | Mårtsbo    | 17.258         | 60.595        | 51                      |
| VIRO    | Virolahti  | 27.555         | 60.539        | 22                      |
| TUOR    | Tuorla     | 22.443         | 60.416        | 41                      |
| METS    | Metsähovi  | 24.395         | 60.217        | 76                      |
| KAR0    | Karlstad   | 13.505         | 59.444        | 83                      |
| LOV0    | Lovö       | 17.830         | 59.340        | 56                      |
| VAN0    | Vänernborg | 12.070         | 58.690        | 135                     |
| NOR0    | Norrköping | 16.250         | 58.590        | 13                      |
| JON0    | Jönköping  | 14.059         | 57.745        | 227                     |
| SPT0    | Borås      | 12.891         | 57.715        | 185                     |
| VIS0    | Visby      | 18.367         | 57.653        | 55                      |
| ONSA    | Onsala     | 11.925         | 57.395        | 9                       |
| OSK0    | Oskarshamn | 16.000         | 57.060        | 120                     |
| HAS0    | Hässleholm | 13.718         | 56.092        | 79                      |

<sup>a</sup>The heights are referenced to the mean sea level.

listed in Table 1. For more details about the networks [see, e.g., *Johansson et al.*, 2002].

[11] The GPS data were analyzed using the GAMIT GPS processing software, developed at the Massachusetts Institute of Technology [*Herring et al.*, 2006]. The software is based on a method referred to as a network solution. This means that many sites are processed together. Since the processing time increases rapidly as the number of sites in the network increases, it is convenient to divide the network into subnetworks and process each one separately [*Lidberg*, 2007]. In our case all SWEPOS sites are processed in one solution and all FinnRef sites in another. Six of the SWEPOS sites have also been included in the FinnRef solution in order to be able to compare the two solutions. All observations are included down to an elevation cutoff angle of 10° and the elevation dependencies of the ZHD and the ZWD were modeled using the mapping functions developed by *Niell* [1996]. In the analysis site coordinates, satellite coordinates, integer ambiguities, and the ZTD are estimated. An elevation-dependent weighting of the GPS observations was used. The weights were determined for each site and each day from a preliminary solution. For details about the data processing, see *Lidberg et al.* [2007] and *Lidberg* [2007].

[12] We chose to use the data from the 10 year period 17 November 1996 to 16 November 2006. The data acquired with SWEPOS from the first 3 years (before 17 November 1996) were not used in order to cover the same time period with all sites. Furthermore, there were a number of antenna

radome changes during 1993–1996 which have a significant impact on the estimated values of the IWV when performing network solutions [*Emardson et al.*, 2000].

#### 4. Deriving the Water Vapor Content From Zenith Total Delays

[13] In order to obtain the ZWD from the estimated ZTD we use the total pressure at the GPS antenna to calculate and subtract the ZHD. A pressure error of 1 hPa results in an error of 2.3 mm in the ZHD, and hence also in the ZWD, which is equivalent to an IWV error of 0.35 kg m<sup>-2</sup>.

[14] The majority of the SWEPOS and FinnRef sites are not equipped with barometers, hence direct pressure measurements are not available. One possible way to obtain pressure data is to use the results from numerical weather models. In this work we have used pressure estimates

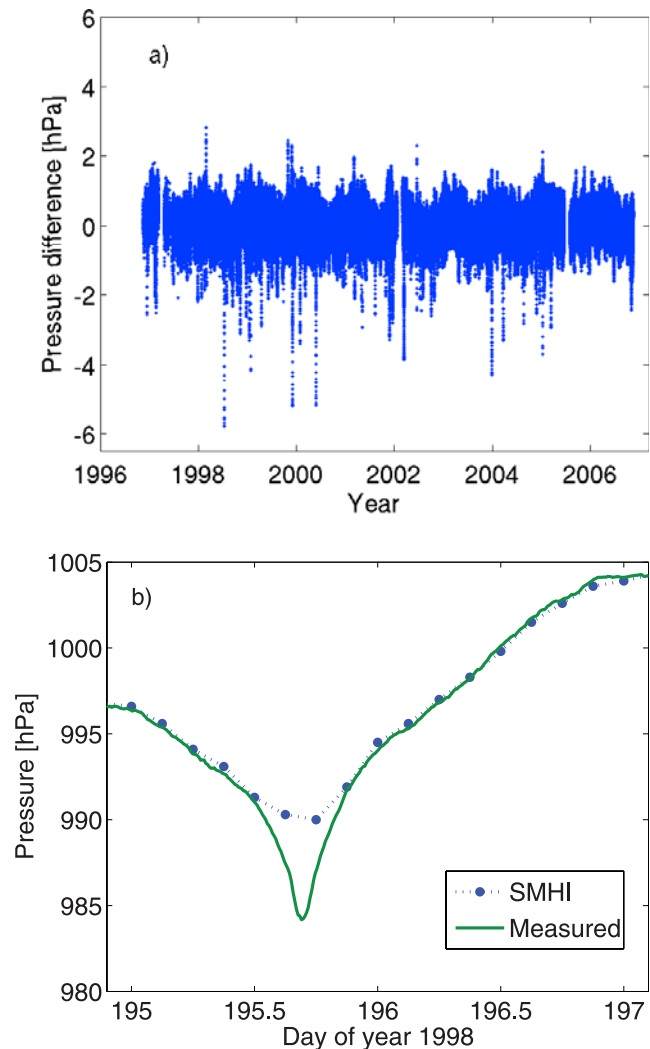


**Figure 2.** Comparison between modeled and measured pressure at the Onsala site. (a) The differences are occasionally large because of the 3 h temporal resolution of the model. (b) The largest difference is caused by rapid variations during the passage of a low-pressure weather system.

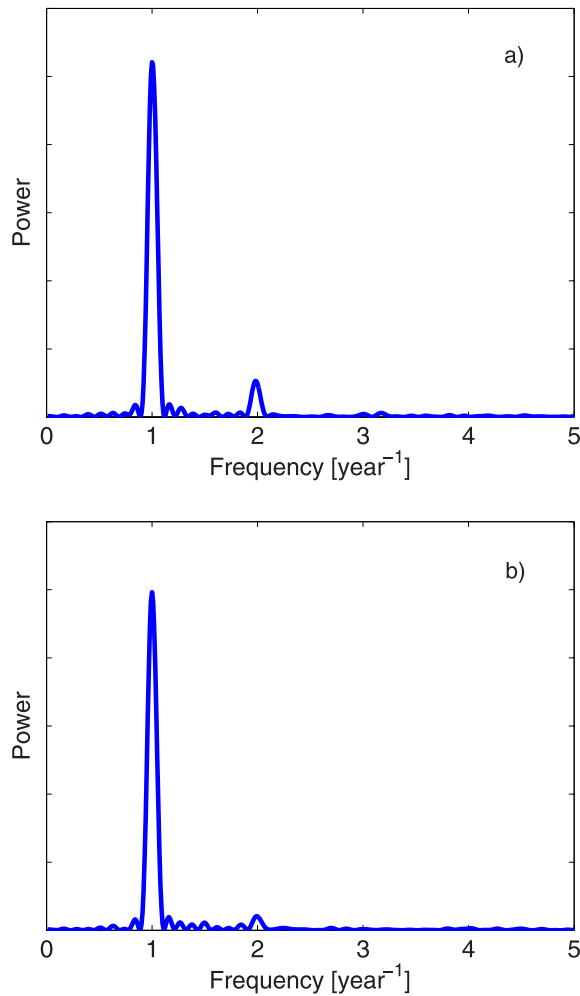


**Figure 3.** Lomb-Scargle periodograms for the IWV time series from (a) Arjeplog and (b) Hässleholm.

obtained from a model used by the Swedish Meteorological and Hydrological Institute (SMHI). However, it is not obvious that the pressure values obtained from this model are accurate enough. For example, *Hagemann et al.* [2003] found that pressure estimated from the ECMWF (European Centre for Medium Range Weather Forecasts) operational analysis did contain too large errors (several hPa). The model used in this work does however have a better resolution than the ECMWF model.

[15] To test the accuracy of the pressure estimates obtained from SMHI, we made a comparison to independent local pressure measurements at the Onsala site (ONSA). The differences between the two time series are shown in Figure 2a. They agree with an RMS difference of 0.42 hPa. We note occasional large differences of several hPa. These are caused by the limited temporal resolution (3 h) of the SMHI model which fails to correctly model the rapid pressure variation associated with a passing low-pressure system. This is illustrated in Figure 2b, showing the period with the largest difference in mid 1998. The estimated linear trend of the difference is  $-0.0074 \text{ hPa a}^{-1}$ . If this were a long-term drift it would introduce an error of  $-0.17 \text{ mm decade}^{-1}$  in the ZWD trend and  $-0.026 \text{ kg m}^{-2} \text{ decade}^{-1}$  in the IWV trend, if not corrected for. However,

we chose not to make any such corrections. It is difficult to determine if it is a true long-term drift in the model or in the barometer measurements. Furthermore, if we assume that the errors are correlated over a few days, the observed drift is comparable to its uncertainty. Given the size of the drift, it is not of large importance for our application because it is significantly below the uncertainties in the linear trends estimated from the GPS data, as we will show below. We conclude that the pressure estimates obtained from SMHI are accurate enough to be used in our study. However, future investigations shall assess the accuracy of the SMHI pressure estimates also at other locations.

[16] The next conversion, from ZWD to IWV will also introduce an error in the trend estimates through any unmodeled trend in the conversion factor. Since the conversion factor (4) depends on a mean temperature of the wet refractivity in the atmosphere, it will be affected by a possible trend in the temperature. An unmodeled mean temperature change of 1 K will introduce an error in the conversion factor of about 0.4%. Assuming that the tem-

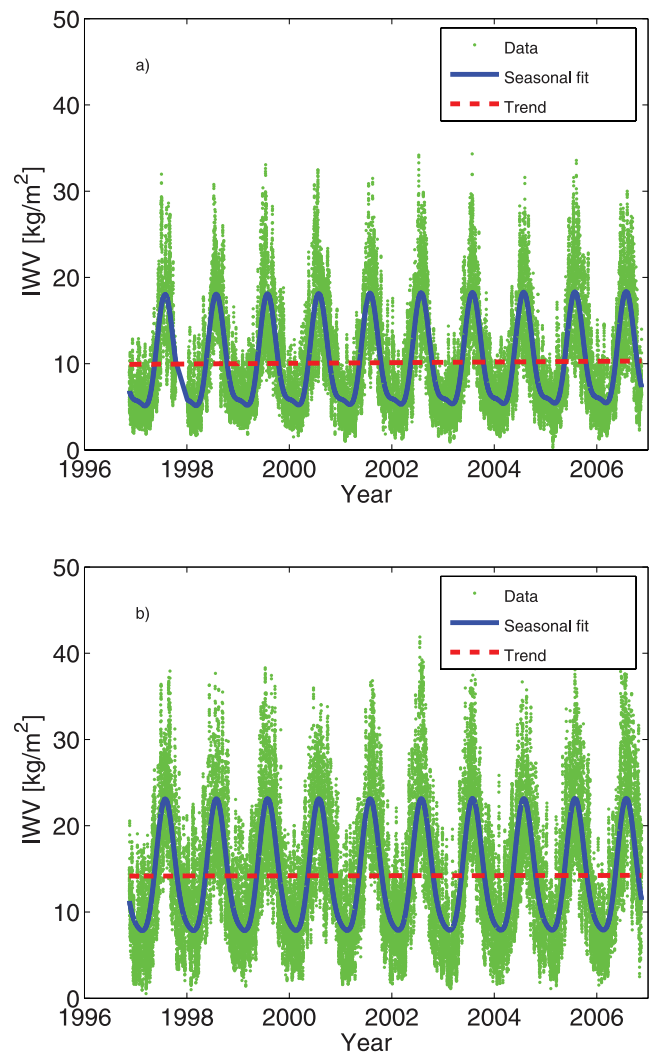


**Figure 4.** IWV time series from (a) Arjeplog and (b) Hässleholm. The straight line is the fitted linear drift, and the periodic function models the seasonal variability in accordance with equation (5).

**Table 2.** Model Parameters Describing the Estimated Long-Term Trends and Annual Systematics in the Equivalent ZWD and the IWV

| Site <sup>a</sup> | Zenith Wet Delay                          |   |                        |                        |                        |                        | Integrated Water Vapor                           |  |                                   |                                   |                                   |                                   | Relative Trend (% decade <sup>-1</sup> ) |
|-------------------|---|---|------------------------|------------------------|------------------------|------------------------|--|--|-----------------------------------|-----------------------------------|-----------------------------------|-----------------------------------|--|
|                   | Mean <sup>b</sup><br>$\ell_{w,0}$<br>(mm) | Trend<br>$a_{\ell w,1}$<br>(mm decade <sup>-1</sup> ) | Annual                 |                        | Semiannual             |                        | Mean <sup>b</sup> $V_0$<br>(kg m <sup>-2</sup> ) | Trend $a_{V1}$<br>(kg m <sup>-2</sup> decade <sup>-1</sup> ) | Annual                            |                                   | Semiannual                        |                                   |  |
|                   |   |   | $a_{\ell w,2}$<br>(mm) | $a_{\ell w,3}$<br>(mm) | $a_{\ell w,4}$<br>(mm) | $a_{\ell w,5}$<br>(mm) |  |  | $a_{V2}$<br>(kg m <sup>-2</sup> ) | $a_{V3}$<br>(kg m <sup>-2</sup> ) | $a_{V4}$<br>(kg m <sup>-2</sup> ) | $a_{V5}$<br>(kg m <sup>-2</sup> ) |  |
| KEVO              | 65.60                                     | 3.83  | -22.4                  | -38.6                  | 9.3                    | 7.5                    | 9.91   | 0.58   | -3.5                              | -6.0                              | 1.5                               | 1.2                               | 5.8                                      |
| KIRO              | 64.22                                     | 2.42  | -19.2                  | -34.6                  | 8.7                    | 9.2                    | 9.72   | 0.37   | -3.0                              | -5.4                              | 1.4                               | 1.4                               | 3.8                                      |
| SODA              | 67.33                                     | 2.31  | -23.0                  | -41.0                  | 8.3                    | 8.4                    | 10.21  | 0.35   | -3.6                              | -6.4                              | 1.3                               | 1.3                               | 3.4                                      |
| ARJ0              | 65.41                                     | 2.54  | -19.7                  | -34.5                  | 8.7                    | 8.0                    | 9.93   | 0.39   | -3.1                              | -5.4                              | 1.4                               | 1.3                               | 3.9                                      |
| OVE0              | 72.79                                     | 2.43  | -22.3                  | -39.9                  | 9.5                    | 9.2                    | 11.05  | 0.37   | -3.5                              | -6.3                              | 1.5                               | 1.4                               | 3.3                                      |
| KUUS              | 64.27                                     | 0.72  | -21.8                  | -41.4                  | 7.3                    | 8.0                    | 9.77   | 0.11   | -3.4                              | -6.5                              | 1.2                               | 1.3                               | 1.1                                      |
| OULU              | 74.18                                     | 2.90  | -24.0                  | -43.3                  | 9.4                    | 8.5                    | 11.29  | 0.45   | -3.7                              | -6.8                              | 1.5                               | 1.3                               | 3.9                                      |
| SKE0              | 78.32                                     | 2.93  | -23.7                  | -42.1                  | 9.2                    | 10.0                   | 11.92  | 0.45   | -3.7                              | -6.6                              | 1.5                               | 1.6                               | 3.7                                      |
| VIL0              | 70.25                                     | 3.85  | -20.3                  | -34.8                  | 8.2                    | 8.1                    | 10.69  | 0.59   | -3.2                              | -5.5                              | 1.3                               | 1.3                               | 5.5                                      |
| ROMU              | 71.68                                     | 0.90  | -22.5                  | -43.1                  | 8.5                    | 8.3                    | 10.92  | 0.15   | -3.5                              | -6.8                              | 1.4                               | 1.3                               | 1.3                                      |
| UME0              | 81.43                                     | 2.00  | -24.5                  | -41.8                  | 9.5                    | 9.1                    | 12.42  | 0.31   | -3.8                              | -6.6                              | 1.5                               | 1.4                               | 2.5                                      |
| OSTO              | 71.21                                     | 2.77  | -20.1                  | -33.8                  | 8.7                    | 7.4                    | 10.86  | 0.43   | -3.2                              | -5.4                              | 1.4                               | 1.2                               | 3.9                                      |
| VAAS              | 79.07                                     | 5.94  | -25.7                  | -41.8                  | 9.3                    | 8.3                    | 12.07  | 0.91   | -4.0                              | -6.6                              | 1.5                               | 1.3                               | 7.5                                      |
| KIVE              | 73.56                                     | 2.76  | -23.7                  | -43.1                  | 8.0                    | 7.6                    | 11.24  | 0.43   | -3.7                              | -6.8                              | 1.3                               | 1.2                               | 3.8                                      |
| JOEN              | 76.68                                     | 3.09  | -24.6                  | -45.4                  | 9.1                    | 10.4                   | 11.72  | 0.48   | -3.9                              | -7.1                              | 1.5                               | 1.6                               | 4.0                                      |
| SUN0              | 83.44                                     | 2.51  | -25.1                  | -41.5                  | 9.3                    | 8.4                    | 12.75  | 0.39   | -3.9                              | -6.6                              | 1.5                               | 1.3                               | 3.0                                      |
| SVE0              | 72.51                                     | 3.33  | -20.9                  | -35.4                  | 8.3                    | 7.7                    | 11.08  | 0.51   | -3.3                              | -5.6                              | 1.3                               | 1.2                               | 4.6                                      |
| OLKI              | 81.76                                     | 5.21  | -25.5                  | -42.0                  | 8.6                    | 8.2                    | 12.51  | 0.81   | -4.0                              | -6.7                              | 1.4                               | 1.3                               | 6.4                                      |
| LEK0              | 74.43                                     | 2.93  | -21.5                  | -35.8                  | 7.2                    | 7.7                    | 11.40  | 0.45   | -3.4                              | -5.7                              | 1.2                               | 1.2                               | 3.9                                      |
| MAR6              | 84.95                                     | 2.56  | -24.3                  | -42.4                  | 8.3                    | 9.2                    | 13.02  | 0.40   | -3.8                              | -6.7                              | 1.3                               | 1.5                               | 3.0                                      |
| VIRO              | 84.23                                     | 4.51  | -24.0                  | -44.5                  | 8.1                    | 10.3                   | 12.91  | 0.70   | -3.8                              | -7.1                              | 1.3                               | 1.6                               | 5.4                                      |
| TUOR              | 79.26                                     | 2.57  | -24.4                  | -41.6                  | 8.4                    | 9.2                    | 12.15  | 0.41   | -3.8                              | -6.6                              | 1.4                               | 1.4                               | 3.2                                      |
| METS              | 80.16                                     | 0.28  | -24.0                  | -42.7                  | 7.9                    | 10.0                   | 12.29  | 0.06   | -3.8                              | -6.8                              | 1.3                               | 1.6                               | 0.4                                      |
| KAR0              | 86.70                                     | 3.83  | -24.5                  | -40.4                  | 7.4                    | 7.5                    | 13.31  | 0.59   | -3.9                              | -6.5                              | 1.2                               | 1.2                               | 4.4                                      |
| LOV0              | 88.43                                     | -1.07   | -24.5                  | -41.1                  | 7.6                    | 9.1                    | 13.57  | -0.16  | -3.9                              | -6.6                              | 1.2                               | 1.4                               | -1.2                                     |
| VAN0              | 86.68                                     | 1.90  | -23.5                  | -38.6                  | 6.6                    | 6.8                    | 13.32  | 0.30   | -3.7                              | -6.2                              | 1.1                               | 1.1                               | 2.2                                      |
| NOR0              | 89.82                                     | 0.03  | -24.9                  | -42.4                  | 7.6                    | 8.6                    | 13.81  | 0.01   | -4.0                              | -6.8                              | 1.2                               | 1.4                               | 0.0                                      |
| JON0              | 85.16                                     | 1.27  | -22.8                  | -39.3                  | 6.2                    | 7.4                    | 13.11  | 0.20   | -3.6                              | -6.3                              | 1.0                               | 1.2                               | 1.5                                      |
| SPT0              | 89.30                                     | 0.82  | -23.5                  | -38.8                  | 6.9                    | 6.8                    | 13.74  | 0.14   | -3.7                              | -6.2                              | 1.1                               | 1.1                               | 0.9                                      |
| VIS0              | 88.65                                     | -1.28   | -24.7                  | -40.9                  | 6.7                    | 8.6                    | 13.65  | -0.19  | -3.9                              | -6.5                              | 1.1                               | 1.4                               | -1.4                                     |
| ONSA              | 88.63                                     | 3.71  | -24.9                  | -40.1                  | 6.8                    | 6.7                    | 13.65  | 0.58   | -4.0                              | -6.4                              | 1.1                               | 1.1                               | 4.2                                      |
| OSK0              | 89.80                                     | -0.93   | -24.3                  | -41.6                  | 6.5                    | 7.5                    | 13.84  | -0.14  | -3.9                              | -6.7                              | 1.1                               | 1.2                               | -1.0                                     |
| HAS0              | 91.85                                     | 0.41  | -24.5                  | -40.3                  | 6.1                    | 6.0                    | 14.17  | 0.07   | -3.9                              | -6.5                              | 1.0                               | 1.0                               | 0.4                                      |

<sup>a</sup>The site names are identified in Table 1 and their locations are seen in the map in Figure 1.

<sup>b</sup>Mean values refers to the time epoch  $t = 0$ , which in this work is 1 January 1997.

perature change over the last decade is less than 1 K, the error in the IWV trends caused by a trend in the conversion factor will be much smaller than the IWV trends we observe (see below). This whole problem can of course be avoided if ZWD is analyzed rather than the IWV. We have, however, done the conversion to IWV using *Emardson et al.* [1998, equation (3)]. This equation is slightly less accurate compared to those using ground temperatures. However, we chose this path rather than risking introducing any trends from such a local point observation.

## 5. Estimation of Linear Trends in IWV

[17] In order to obtain the linear trends from the GPS time series we need to consider the annual variations in water vapor, especially if there are gaps in the time series (or if the length of the investigated period would not be an integer number of years). In order to investigate how many terms in a Fourier expansion that are needed in order to describe the annual variation of the IWV (annual term, semiannual term etc.), and also to investigate if there are any other periodic variations on time scales  $\sim 1$  year, we calculated the Lomb-Scargle periodograms [*Hocke, 1998*] from the time series. Two examples are shown in Figure 3. We can clearly see a peak for the annual period, and also one much smaller at the semiannual period. No other significant peaks are seen,

indicating that it is sufficient to use an annual and a semiannual term to describe the seasonal variations. We note that the semiannual term is relatively stronger at the Arjeplog site, in the north of Sweden, compared to the results for the Hässleholm site in the south.

[18] We also investigated to use a logarithmic scale in the analysis, i.e., studying  $\log(V + \Delta)$  instead of in  $V$  because this may suppress the semiannual term. The constant  $\Delta$  should be chosen so that the variability of  $\log(V + \Delta)$  is relatively constant over the year. We found that this approach indeed decreased the semiannual term, especially when a  $\Delta$  close to zero is used. However, the semiannual term was generally still significant and needed to be estimated. Furthermore, there were only small differences in the trends estimated using a logarithmic scale or a linear scale (at the most these differed by  $0.1 \text{ kg m}^{-2} \text{ decade}^{-1}$ ). Hence, we have used IWV in a linear scale when estimating the trends but note that a logarithmic scale may be investigated further using other data sets.

[19] On the basis of the results from the periodograms, the following model is used with the ZWD and the IWV time series:

$$V = V_0 + a_1 t + a_2 \sin(2\pi t) + a_3 \cos(2\pi t) + a_4 \sin(4\pi t) + a_5 \cos(4\pi t) \quad (5)$$

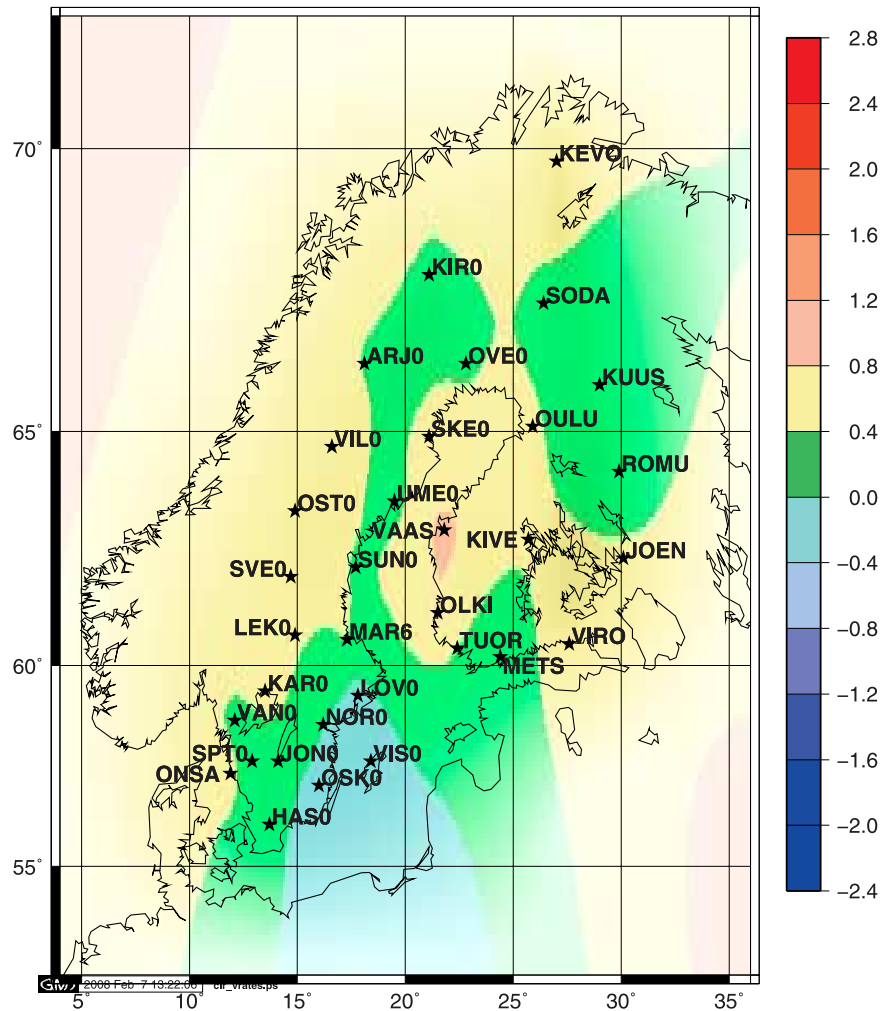


**Figure 5.** Estimated IWV trends (in  $\text{kg m}^{-2} \text{decade}^{-1}$ ) in Sweden and Finland for the period 17 November 1996 to 16 November 2006.

where  $t$  is the time in years and the coefficients  $V_0$ ,  $a_1$ ,  $a_2$ ,  $a_3$ ,  $a_4$ , and  $a_5$ , are estimated using the method of least squares.

[20] Two examples of the original time series and the fitted models are presented in Figure 4. As seen the fit follows the seasonal pattern well, however there are also variations on time scales of a few weeks or less which are of course not described by the model.

[21] We have estimated trends as well as the other model parameters in both the ZWD and the IWV for the different sites shown in Figure 1. The results are given in Table 2. The average ZWD/IWV typically is larger for the sites in the south compared to the sites in the north, as expected. Furthermore, the seasonal variations show more water vapor in the summer compared to the winter, also as expected. The semiannual terms are little bit larger at the northern sites because the period of higher IWV in summer is shorter at the northern sites than at the southern ones (see Figure 4). The ratio between the amplitudes of the annual and semiannual terms agree with what is expected from the Lomb-Scargle periodograms.

[22] When studying the values of the estimated trends we note that the relative values of the ZWD trends and the IWV

trends are almost identical. This is expected because the conversion algorithm used to derive the IWV from the ZWD does only include the site latitude and the time of the year. Hence, in Table 2 we give only one relative trend, valid for both the ZWD and the IWV. In the following we focus on the estimated trends in the IWV.

[23] The trends in the IWV for the full 10 year time period fall in the range from  $-0.2$  to  $+1.0 \text{ kg m}^{-2} \text{decade}^{-1}$ . Figure 5 shows the geographical pattern of these trends. The trends at sites located close to each other are similar and there are differences in the trends at sites in the northern part of the area compared to sites in the southern part. The trends are largest for the northwestern sites and around the site Vaasa, while the trends at the sites in the southeast of Sweden are slightly negative.

[24] The sensitivity of the trends to the selected time period is demonstrated in Figure 6 and in Table 3, where the trends obtained using only the first 8 years or the last 8 years of the period are shown. The trends obtained using data from only the last 8 years are much smaller than those obtained using the first 8 years, or the whole 10 year period. The reason is that a 10 (or 8) year period is too short. A very wet or dry year in the beginning or the end of the period will

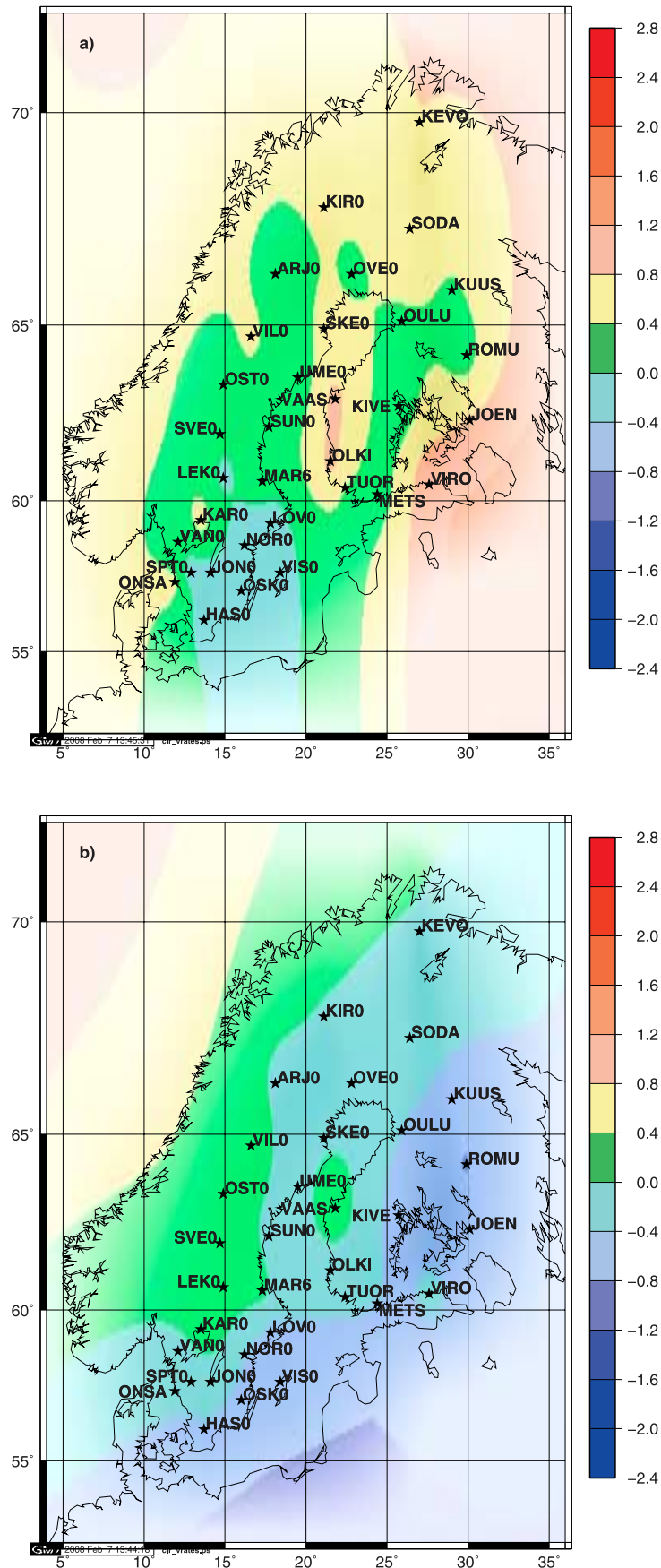


**Figure 6.** Estimated IWV trends (in  $\text{kg m}^{-2} \text{decade}^{-1}$ ) using subsets of the available 10 years of data: (a) 17 November 1996 to 16 November 2004 and (b) 17 November 1998 to 16 November 2006.

**Table 3.** IWV Trends Obtained From the Two 8-Year Periods 1996–2004 and 1998–2006 and From Summer and Winter Data

| Site <sup>a</sup> | Trend  |  |   |   |
|-------------------|--|--|---|---|
|                   | 1996–2004<br>(kg m <sup>-2</sup><br>decade <sup>-1</sup> ) | 1998–2006<br>(kg m <sup>-2</sup><br>decade <sup>-1</sup> ) | Summer<br>(kg m <sup>-2</sup><br>decade <sup>-1</sup> ) | Winter<br>(kg m <sup>-2</sup><br>decade <sup>-1</sup> ) |
| KEVO              | 0.79   | -0.05  | 1.02  | -0.01   |
| KIRO              | 0.46   | -0.03  | 0.78  | -0.05   |
| SODA              | 0.56   | -0.22  | 0.84  | -0.11   |
| ARJ0              | 0.18   | -0.09  | 0.78  | -0.04   |
| OVE0              | 0.33   | -0.17  | 0.67  | 0.13  |
| KUUS              | 0.36   | -0.53  | 0.89  | -0.70   |
| OULU              | 0.37   | -0.39  | 1.40  | -0.98   |
| SKE0              | 0.53   | -0.09  | 0.97  | -0.06   |
| VIL0              | 0.51   | 0.23   | 1.04  | 0.17  |
| ROMU              | 0.22   | -0.84  | 1.28  | -0.93   |
| UME0              | 0.10   | -0.15  | 0.78  | -0.10   |
| OSTO              | 0.11   | 0.17   | 0.82  | 0.10  |
| VAAS              | 0.92   | 0.34   | 1.89  | 0.01  |
| KIVE              | 0.15   | -0.59  | 1.66  | -0.60   |
| JOEN              | 0.83   | -0.49  | 1.10  | -0.22   |
| SUN0              | 0.14   | -0.12  | 0.89  | -0.04   |
| SVE0              | 0.10   | 0.31   | 0.83  | 0.28  |
| OLKI              | 0.93   | -0.26  | 1.82  | -0.39   |
| LEK0              | -0.10  | 0.32   | 0.73  | 0.25  |
| MAR6              | 0.31   | 0.11   | 0.82  | -0.00   |
| VIRO              | 1.17   | -0.34  | 1.30  | -0.13   |
| TUOR              | 0.40   | -0.32  | 1.18  | -0.43   |
| METS              | 0.18   | -0.40  | 0.63  | -0.49   |
| KAR0              | 0.61   | 0.20   | 0.85  | 0.40  |
| LOV0              | -0.34  | -0.52  | 0.03  | -0.30   |
| VAN0              | 0.02   | -0.16  | 0.42  | 0.21  |
| NOR0              | -0.25  | -0.39  | 0.19  | -0.11   |
| JON0              | -0.12  | -0.14  | 0.33  | 0.09  |
| SPT0              | -0.18  | -0.31  | 0.39  | -0.07   |
| VIS0              | -0.18  | -0.58  | -0.19   | -0.16   |
| ONSA              | 0.52   | -0.33  | 0.73  | 0.46  |
| OSK0              | -0.38  | -0.53  | -0.15   | -0.06   |
| HAS0              | -0.14  | -0.44  | 0.36  | -0.17   |

<sup>a</sup>The site names are identified in Table 1, and their locations are seen in the map in Figure 1.

have a significant impact on the estimated trends. We can however note that the overall pattern with the smallest trends in southeast Sweden and larger trends in northwest and around Vaasa is seen for all periods.

[25] A similar effect, in terms of sensitivity, is seen in Figure 7 and Table 3 where we compare the results obtained using only data from the summer (April–September) or the winter (October–March). There are large differences between the seasons, with larger trends in the summer period. This may be an effect caused by the different periods analyzed (similar as in Figure 6), or an actual seasonal difference in trend which will also be seen in future longer-term trends for summer and winter data.

[26] For the sites included in both the SWEPOS and the FinnRef solutions it is possible to compare the estimated IWV to check if they are consistent. Such a comparison is shown in Figure 8 for the Umeå site. There is a mean difference between the SWEPOS and the FinnRef solution of 0.25 kg m<sup>-2</sup> and an RMS scatter of 0.5 kg m<sup>-2</sup> around this mean. The trend in the difference is for this period 0.02 kg m<sup>-2</sup> decade<sup>-1</sup>. The results are similar for the other overlapping sites: a mean difference in IWV of 0.2–0.3 kg m<sup>-2</sup> and trends in the differences of less than 0.09 kg m<sup>-2</sup> decade<sup>-1</sup>. This demonstrates that the estimated trends are not significantly affected by the network used.

However, the fact that there is an average difference in IWV between different network solutions shows that estimates from different networks should not be mixed when estimating a trend. For example, an estimated trend for the Umeå site based on the FinnRef solution for the first 5 years and the SWEPOS solution for the last 5 years, will introduce an error in the trend of 0.38 kg m<sup>-2</sup> decade<sup>-1</sup>. This would be a significant error since it is slightly larger than the observed trend at Umeå (0.31 kg m<sup>-2</sup> decade<sup>-1</sup>).

## 6. Estimation of Trend Uncertainties

[27] The formal uncertainties in the linear trends can be estimated by statistical methods. If we assume that the IWV errors are white noise with variances equal to those estimated in the GAMIT solution, the uncertainty of the trend will be less than 0.03 kg m<sup>-2</sup> decade<sup>-1</sup>. However, this uncertainty will only give information on how the estimated trend differs from what would be estimated if the IWV did not contain any errors. It will not say anything about how significant the trend is, if it can or cannot be concluded from the trends that there is a long-term increase or decrease in IWV. To get an uncertainty that can be used for that purpose we also need to consider that the true short-term variability (at time scales up to several weeks) in the IWV is not modeled by equation (5), and hence when assessing the significance of the trend these variations should be considered as noise.

[28] The statistical properties of the IWV model errors, i.e., including both short-term variability in IWV and errors from the GPS processing, can be estimated from the residuals after the fit of the IWV to the model in (5). If we (incorrectly) assume that the observed deviations from the models are well described by white noise, we obtain 1- $\sigma$  uncertainties of less than 0.1 kg m<sup>-2</sup> decade<sup>-1</sup>. However, the deviations are correlated over several days. To take these correlations into account, we need a model to describe the covariance between IWV values  $V_1$  and  $V_2$  observed at the time epochs  $t_1$  and  $t_2$ . After testing several different models for the covariances, it was found that the following expression described the covariances sufficiently well:

$$\text{Cov}[V_1(t_1), V_2(t_2)] = k_1 2^{-|t_1-t_2|/T_1} + k_2 2^{-|t_1-t_2|/T_2} \quad (6)$$

[29] To obtain the parameters  $k_1$ ,  $k_2$ ,  $T_1$ , and  $T_2$  we first calculated the covariance of the residuals as function of time. These were then used in a nonlinear least squares fit (using the function lsqcurvefit in MATLAB) to obtain the parameters of the model of (6). The covariance matrix  $C$  for the observations can then be computed from the covariance model. The formal 1- $\sigma$  uncertainties of the estimated parameters in the model (5) are calculated by:

$$C_x = (M^T M)^{-1} M^T C M (M^T M)^{-1} \quad (7)$$

where  $M$  is the design matrix of the linear system of equations based on equation (5), and  $C_x$  is the covariance matrix for the errors in the estimated parameters.

[30] Figure 9 shows both the covariance calculated using the residuals as well as the model fits for the two sites Arjeplog and Hässleholm. Also shown in these plots is the

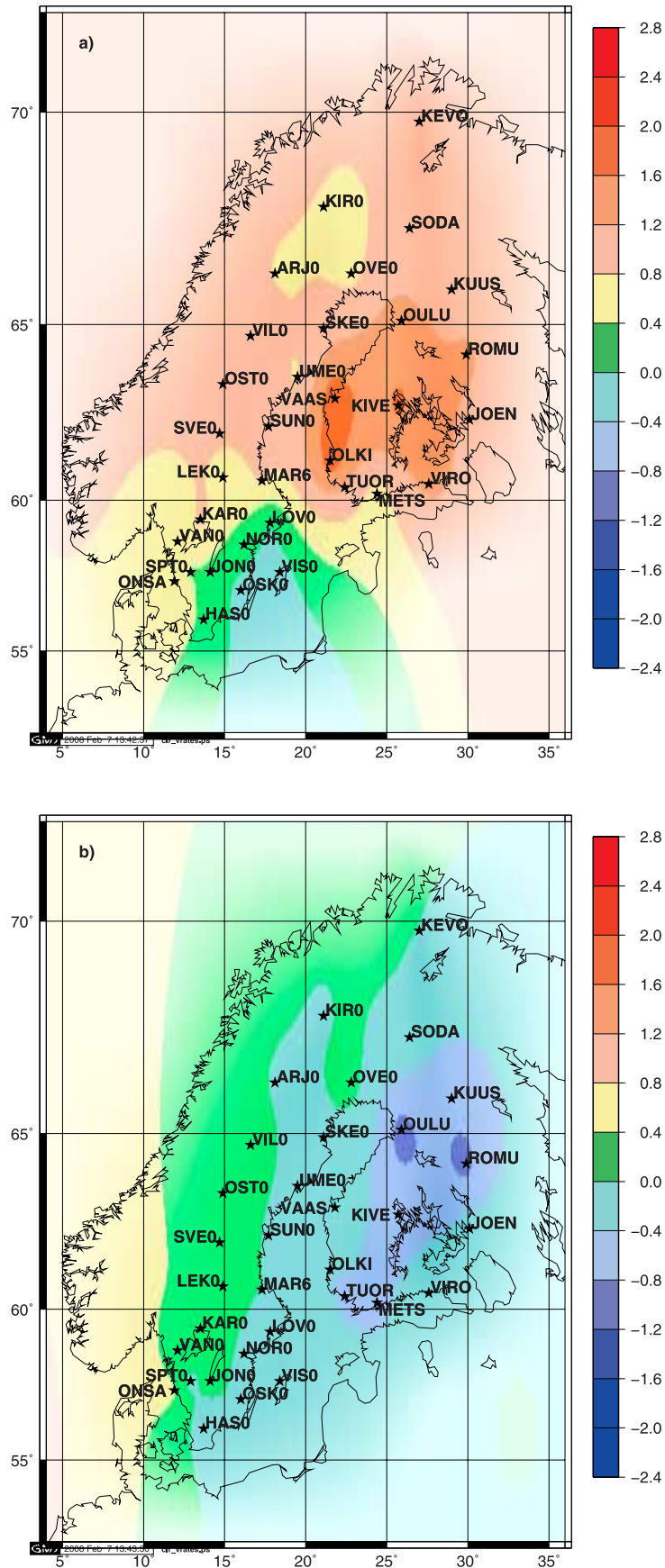
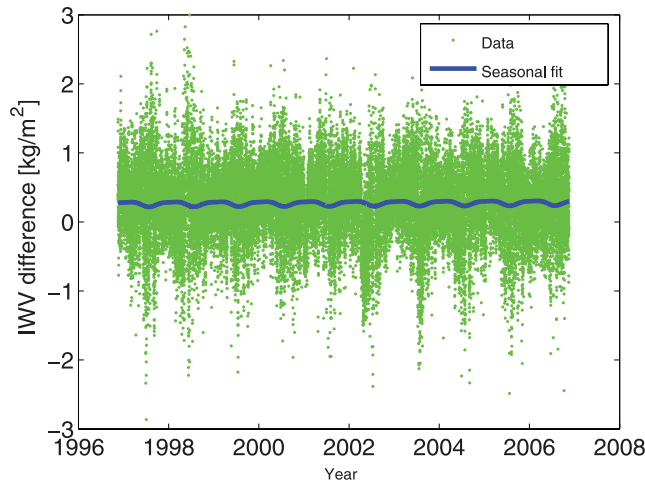


Figure 7. Estimated IWV trends (in kg m<sup>-2</sup> decade<sup>-1</sup>) using seasonal data: (a) summer data and (b) winter data.



**Figure 8.** The difference between the IWV estimated in the SWEPOS solution and in the FinnRef solution, for the Umeå site.

model result obtained if only one term is used in the covariance model. When taking these covariances into account, using the two term model described by (6), the formal 1- $\sigma$  error is approximately 0.4–0.5 kg m<sup>-2</sup> decade<sup>-1</sup> for the 10 year long data set, i.e., at least a factor of four larger than when assuming the deviations to be white noise. A similar study, using 8 years of GPS data from South Africa, resulted in an increase by a factor of two describing the deviations with an ARMA(1, 1) model [Combrink *et al.*, 2007]. The weather conditions in South Africa are however significantly different from the typical situation in Sweden and Finland.

[31] The obtained model parameters for all sites are shown in Table 4. As seen the covariances for shorter time scales are larger for the sites in the south (as seen by the  $k_1$  parameter). The covariances over longer time scales (described by  $k_2$  and  $T_2$ ) differs less between the different locations.

[32] Systematic errors introduced in the GPS data must also be taken into account when estimating trends over time scales of many years. We do not make any attempt to model these effects in this work, but rather recommend that this is important to study in the future as the time series of GPS data from different areas, with different climate, become available. We can today identify the following sources of systematic errors:

[33] 1. Unmodeled delays which have a dependence of the elevation angle are of fundamental importance since such a dependence is used, through the mapping functions of the hydrostatic and wet atmospheric delays, to estimate the ZTD. Errors in the mapping functions will therefore add different bias-type effects depending on the elevation cutoff angle [Stoew *et al.*, 2007]. Phase center variations of the satellite and ground antennas will also add biases depending on the distribution of observations at different elevation angles. A constant bias is acceptable when searching for trends but this implies that the distribution of observations must remain stable of the entire time period studied. Such a requirement will not be fulfilled if there are changes in the GPS satellite constellation over time. Furthermore, the bias

will change if a satellite is replaced with another satellite having an antenna with a different phase center pattern [Schmid and Rothacher, 2003], or similarly if the receiver antenna is replaced by an antenna of a different type. An obvious improvement, although not done in this analysis, is therefore to model the phase center variations of the individual satellite and ground antennas [Schmid *et al.*, 2007]. In spite of the possibility to correct for antenna effects the interaction with the electromagnetic environment at the site is still a potential problem [Granström, 2006]. Surface wetness, rain, and snow are likely to affect multipath and scattering effects at a receiver site. Other changes such as adding or removing a reflecting object close to a receiver site or changing the radome can have a serious impact. For example, as shown by Emardson *et al.* [2000] and Gradinarsky *et al.* [2002] changing an antenna radome to a different type can introduce an offset of more than 1 kg m<sup>-2</sup> in the IWV.

[34] 2. Errors in the reference frame can propagate into the IWV estimates. For example, Steigenberger *et al.* [2007]

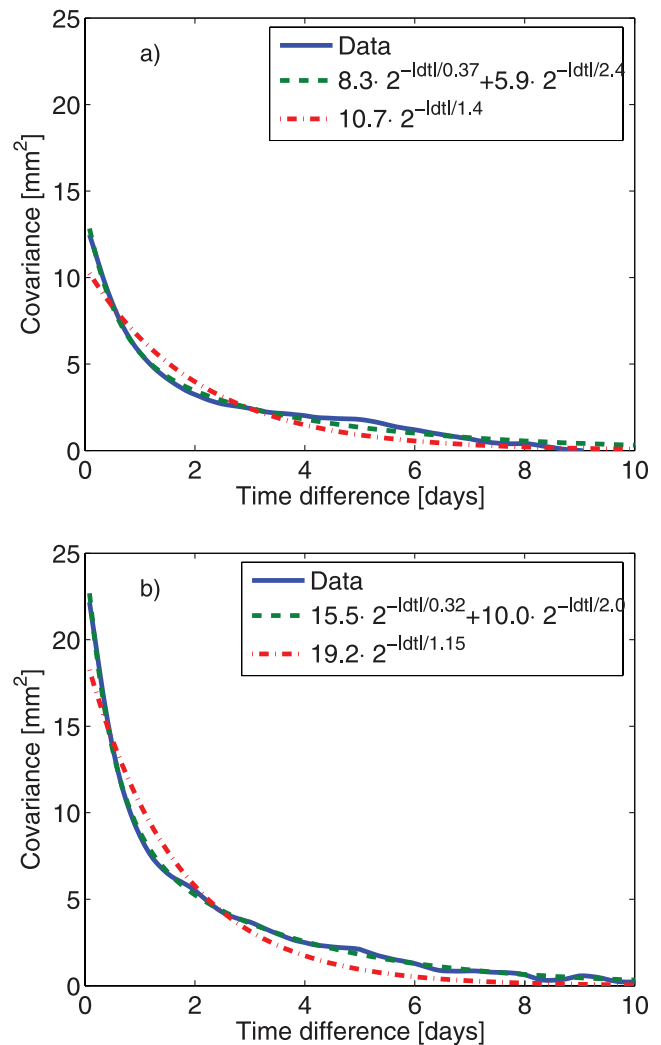


**Figure 9.** Covariance of IWV time series from (a) Arjeplog and (b) Hässleholm. The solid line is the observed covariance. The dash-dotted and the dotted lines are the one and the two term models, respectively.

**Table 4.** Model Parameters Describing the Temporal Correlation of the Deviation Between the Observed and the Modeled IWV

| Site <sup>a</sup> | $k_1$ | $k_2$ | $T_1$ (days) | $T_2$ (days) |
|-------------------|-------|-------|--------------|--------------|
| KEVO              | 7.6   | 8.0   | 0.36         | 2.43         |
| KIRO              | 6.6   | 6.0   | 0.36         | 2.19         |
| SODA              | 9.0   | 6.9   | 0.44         | 2.73         |
| ARJ0              | 8.3   | 5.9   | 0.37         | 2.36         |
| OVE0              | 9.5   | 7.2   | 0.37         | 2.33         |
| KUUS              | 10.1  | 7.0   | 0.38         | 2.65         |
| OULU              | 12.6  | 9.6   | 0.37         | 2.62         |
| SKE0              | 12.7  | 7.4   | 0.38         | 2.57         |
| VIL0              | 10.7  | 5.2   | 0.42         | 2.63         |
| ROMU              | 10.5  | 7.6   | 0.34         | 2.58         |
| UME0              | 14.6  | 7.6   | 0.37         | 2.78         |
| OST0              | 11.5  | 4.8   | 0.39         | 3.08         |
| VAAS              | 15.7  | 7.8   | 0.37         | 3.40         |
| KIVE              | 12.7  | 6.5   | 0.39         | 3.10         |
| JOEN              | 12.5  | 9.7   | 0.36         | 3.09         |
| SUN0              | 16.5  | 6.3   | 0.40         | 3.42         |
| SVE0              | 12.7  | 4.3   | 0.41         | 3.81         |
| OLKI              | 17.3  | 6.8   | 0.37         | 3.55         |
| LEK0              | 14.0  | 4.7   | 0.37         | 3.87         |
| MAR6              | 17.4  | 5.7   | 0.40         | 3.80         |
| VIRO              | 15.9  | 9.2   | 0.36         | 2.79         |
| TUOR              | 18.0  | 6.3   | 0.38         | 3.84         |
| METS              | 15.9  | 8.1   | 0.35         | 3.06         |
| KAR0              | 17.3  | 7.0   | 0.36         | 3.28         |
| LOV0              | 17.2  | 6.5   | 0.39         | 3.42         |
| VAN0              | 17.1  | 7.1   | 0.36         | 2.83         |
| NOR0              | 17.3  | 7.5   | 0.38         | 3.12         |
| JON0              | 15.5  | 7.6   | 0.33         | 2.45         |
| SPT0              | 16.1  | 8.0   | 0.35         | 2.50         |
| VIS0              | 16.8  | 7.3   | 0.41         | 2.84         |
| ONSA              | 19.2  | 7.7   | 0.40         | 2.74         |
| OSK0              | 14.8  | 9.8   | 0.31         | 2.16         |
| HAS0              | 15.5  | 10.0  | 0.32         | 2.03         |

<sup>a</sup>The site names are identified in Table 1 and their locations are seen in the map in Figure 1.

reported a varying trend between the ZTD estimated by the IGS (International GNSS Service) and their reference solution. The variations in the trend coincided with the different ITRFs (International Terrestrial Reference Frames) used in the different periods. However, in our analysis this effect can be expected to be low since we estimated both station coordinates and satellites orbits with relatively loose constraints (5–10 cm for well established sites and up to tens of meters for other sites).

[35] 3. Higher-order terms in the correction for the ionospheric delay will introduce an effect which is likely to correlate with the 11 year solar cycle. Results by *Hernández-Pajares et al.* [2007], using data from 2002 to 2003 close to a solar maximum, show a correction to the vertical coordinate of the order of a couple of millimeters due to second-order effects. There will be an effect on the IWV estimate through the correlation between errors in the vertical coordinate and the atmospheric delay. This result, however, indicates that it is below the  $0.1 \text{ kg m}^{-2}$  level.

[36] Many of these systematic effects are worse for observations at low-elevation angles. Including these observations strengthens the geometry and reduces the formal uncertainties of individual coordinate and atmospheric estimates. The formal uncertainties of the ZTDs are, however, not the limiting factor for the trend uncertainties in our application. The highest priority is to have long time series with as small systematic effects as possible and it is important to note that the  $10^\circ$  elevation cutoff angle used

in this analysis may not be the optimum in order to minimize the influence of systematic errors.

## 7. Discussion

[37] When assessing linear trends in IWV it is also important to consider variations in the IWV on time scales of a few years caused by, e.g., volcano eruptions and El Niño. This is especially important when the time series are as short as in this study. As shown by *Trenberth et al.* [2005] periods of El Niño cause a significant increase in the global IWV. However, effects of El Niño are mostly important for regions around the equator, hence they may not have significantly affected our results.

[38] The trends estimated in this work are generally slightly lower than those found by *Gradinarsky et al.* [2002] for the SWEPOS sites. A likely reason for this is that they used another period (August 1993 to December 2000). Also, the changes to the SWEPOS sites during 1993–1996 might have affected their results, and they used another processing strategy for the GPS data, Precise Point Positioning (PPP). The advantage of using PPP instead of a network solution is that a systematic error at one site will only affect the IWV at that site, while all sites in the network might be affected in a network solution. The potential problem with PPP is that it needs a priori estimating of the satellite orbits (e.g., by a network solution) and any systematic errors in these will affect the results. We will investigate the differences between IWV estimated by these two strategies in more detail in the future.

[39] The obtained trends could be compared to the trends obtained using other methods. However, other published investigations use different time periods so the results are not directly comparable. *Ross and Elliott* [2001] found a trend of  $-0.05 \text{ kg m}^{-2} \text{ decade}^{-1}$  for the whole of Europe and the period 1973–1995 (using radiosonde data). *Trenberth et al.* [2005] used ERA40 and the NCEP reanalysis to obtain the global distribution of the IWV trends. For the region around Sweden and Finland the trends from both these reanalysis were found to be between  $-0.5$  and  $+0.5 \text{ kg m}^{-2} \text{ decade}^{-1}$  for the period 1988–2001.

## 8. Conclusions and Outlook

[40] We have used a 10 year long data set of GPS observations acquired by 33 receiver sites in Finland and Sweden. When fitting a seasonal model to the inferred time series of IWV we obtain linear trends in the range from  $-0.2$  to  $+1.0 \text{ kg m}^{-2} \text{ decade}^{-1}$ . We find, as expected, that a 10 year period is too short to obtain stable values for the estimated trends. The patterns seen across the studied area are however realistic and no GPS site stands out with a significantly different result. We conclude that as the time series become longer it will become possible to assess the systematic drifts in the GPS data in much more detail.

[41] We find that taking the temporal correlations of the IWV deviations from the model into account the formal uncertainties in the trends are of the order of  $0.4 \text{ kg m}^{-2} \text{ decade}^{-1}$ , a factor of four larger compared to assuming the model deviations to be white noise. We have shown that the estimated uncertainties of the trends are mostly due to the natural variability in the IWV and not so

much due to random errors in the IWV estimates. Hence, for investigation of climate trends it is probably not that important to use a low-elevation cutoff angle in the GPS data analysis. Several systematic errors affecting the trends are mostly important for low-elevation angle observations, hence by using a high-elevation cutoff angle these effects can be decreased. However, the systematic errors affecting observations at high-elevation angles will have a larger impact on the estimated IWV. In the future we will investigate the impact of using a higher-elevation cutoff angle.

[42] We will continue to investigate trends in IWV estimated from GPS. It would be interesting to look at data from regions where other investigations have seen significant IWV trends. For example, the results of *Ross and Elliott* [2001] and *Trenberth et al.* [2005] indicate that the trends in the Pacific Ocean are much more significant than in Europe.

[43] **Acknowledgments.** We are grateful to Martin Lidberg at Chalmers and Lars Mueller at the SMHI for providing the ZTD time series and the ground meteorological data, respectively. The maps were produced using the Generic Mapping Tools (GMT) [Wessel and Smith, 1998]. The ongoing research project "Long Term Water Vapour Measurements Using GPS for Improvement of Climate Modelling" is funded by the Swedish Governmental Agency for Innovation Systems (VINNOVA).

## References

- Bengtsson, L., S. Hagemann, and K. I. Hodges (2004), Can climate trends be calculated from reanalysis data?, *J. Geophys. Res.*, *109*, D11111, doi:10.1029/2004JD004536.
- Bevis, M., S. Businger, T. Herring, C. Rocken, R. Anthes, and R. Ware (1992), GPS meteorology: Remote sensing of atmospheric water vapor using the Global Positioning System, *J. Geophys. Res.*, *97*, 15,787–15,801.
- Buehler, S. A., A. von Engel, E. Brocard, V. O. John, T. Kuhn, and P. Eriksson (2006), Recent developments in the line-by-line modeling of outgoing longwave radiation, *J. Quant. Spectrosc. Radiat. Transfer*, *98*(3), 446–457, doi:10.1016/j.jqsrt.2005.11.001.
- Combrink, A., M. S. Bos, R. M. Fernandes, W. L. Combrink, and C. L. Merry (2007), On the importance of proper noise modelling for long-term precipitable water vapour trend estimations, *S. Afr. J. Geol.*, *110*, 211–218.
- Davis, J. L., T. A. Herring, I. I. Shapiro, A. E. E. Rogers, and G. Elgered (1985), Geodesy by radio interferometry: Effects of atmospheric modeling errors on estimates of baseline length, *Radio Sci.*, *20*, 1593–1607.
- Elgered, G. (1993), Tropospheric radio-path delay from ground based microwave radiometry, in *Atmospheric Remote Sensing by Microwave Radiometry*, edited by M. Janssen, chap. 5, pp. 215–258, John Wiley, New York.
- Elliott, W. P., R. J. Ross, and W. H. Blackmore (2002), Recent changes in NWS upper-air observations with emphasis on changes from VIZ to Vaisala radiosondes, *Bull. Am. Meteorol. Soc.*, *83*, 1003–1017.
- Emardson, T. R., and H. J. P. Derks (2000), On the relation between the wet delay and the integrated precipitable water vapour in the European atmosphere, *Meteorol. Appl.*, *7*, 61–68.
- Emardson, T. R., G. Elgered, and J. M. Johansson (1998), Three months of continuous monitoring of atmospheric water vapour with a network of Global Positioning System receivers, *J. Geophys. Res.*, *103*, 1807–1820.
- Emardson, T., J. Johansson, and G. Elgered (2000), The systematic behavior of water vapor estimates using four years of GPS observations, *IEEE Trans. Geosci. Remote Sens.*, *38*(1), 324–329.
- Gradinarsky, L. P., J. Johansson, H. R. Bouma, H.-G. Scherneck, and G. Elgered (2002), Climate monitoring using GPS, *Phys. Chem. Earth*, *27*, 225–340.
- Granström, C. (2006), Site-dependent effects in high-accuracy applications of GNSS, *Rep. 13L*, Dep. of Radio and Space Sci., Chalmers Univ. of Technol., Göteborg, Sweden.
- Gutman, S., S. Sahm, S. Benjamin, B. Schwartz, K. Holub, J. Stewart, and T. L. Smith (2004), Rapid retrieval and assimilation of ground based GPS precipitable water observations at the NOAA Forecast Systems Laboratory: Impact on weather forecasts, *J. Meteorol. Soc. Jpn.*, *82*(1B), 351–360.
- Haas, R., G. Elgered, L. Gradinarsky, and J. Johansson (2003), Assessing long term trends in the atmospheric water vapor content by combining data from VLBI, GPS, radiosondes and microwave radiometry, in *16th Working Meeting On European VLBI for Geodesy and Astrometry*, edited by W. Schwegmann and V. Thorand, pp. 279–288, Bundesamt für Kartogr. und Geod., Frankfurt, Germany.
- Hagemann, S., L. Bengtsson, and G. Gendt (2003), On the determination of atmospheric water vapor from GPS measurements, *J. Geophys. Res.*, *108*(D21), 4678, doi:10.1029/2002JD003235.
- Hernández-Pajares, M., J. M. Juan, J. Sanz, and R. Orús (2007), Second-order ionospheric term in GPS: Implementation and impact on geodetic estimates, *J. Geophys. Res.*, *112*, B08417, doi:10.1029/2006JB004707.
- Herring, T. A., R. W. King, and S. C. McClusky (2006), Introduction to GAMIT/GLOBK, technical report, Dep. of Earth, Atmos., and Planet. Sci., Mass. Inst. of Technol., Cambridge. (Available at [http://chandler.mit.edu/~simon/gtgk/Intro\\_GG\\_10.3.pdf](http://chandler.mit.edu/~simon/gtgk/Intro_GG_10.3.pdf))
- Hocke, K. (1998), Phase estimation with Lomb-Scargle periodogram method, *Ann. Geophys.*, *16*, 356–358.
- Intergovernmental Panel on Climate Change (2007), *Climate Change 2007: The Physical Science Basis-Contribution of Working Group I to the Fourth Assessment Report of the Intergovernmental Panel on Climate Change*, Cambridge Univ. Press, Cambridge, U.K.
- Jin, S., J.-U. Park, J.-H. Cho, and P.-H. Park (2007), Seasonal variability of GPS-derived zenith tropospheric delay (1994–2006) and climate implications, *J. Geophys. Res.*, *112*, D09110, doi:10.1029/2006JD007772.
- Johansson, J. M., et al. (2002), Continuous GPS measurements of postglacial adjustment in Fennoscandia: I. Geodetic results, *J. Geophys. Res.*, *107*(B8), 2157, doi:10.1029/2001JB000400.
- Lidberg, M. (2007), Geodetic reference frames in presence of crustal deformations, Ph.D. thesis, Dep. of Radio and Space Sci., Chalmers Univ. of Technol., Göteborg, Sweden.
- Lidberg, M., J. M. Johansson, H.-G. Scherneck, and J. L. Davis (2007), An improved and extended GPS-derived 3D velocity field of the glacial isostatic adjustment (GIA) in Fennoscandia, *J. Geod.*, *81*(3), 213–230, doi:10.1007/s00190-006-0102-4.
- Mears, C., B. D. Santer, F. J. Wentz, K. Taylor, and M. Wehner (2007), Relationship between temperature and precipitable water changes over tropical oceans, *Geophys. Res. Lett.*, *34*, L24709, doi:10.1029/2007GL031936.
- Niell, A. (1996), Global mapping functions for the atmosphere delay at radio wavelengths, *J. Geophys. Res.*, *101*(B2), 3227–3246.
- Ross, R. J., and W. P. Elliott (1996), Tropospheric water vapor climatology and trends over North America: 1973–93, *J. Clim.*, *9*(12), 3561–3574.
- Ross, R. J., and W. P. Elliott (2001), Radiosonde-based Northern Hemisphere tropospheric water vapor trends, *J. Clim.*, *14*(7), 1602–1611.
- Schmid, R., and M. Rothacher (2003), Estimation of elevation-dependent satellite antenna phase center variations of GPS satellites, *J. Geod.*, *77*(7–8), 440–446.
- Schmid, R., P. Steigenberger, G. Gendt, M. Ge, and M. Rothacher (2007), Generation of a consistent absolute phase center correction model for GPS receiver and satellite antennas, *J. Geod.*, *81*(12), 781–798, doi:10.1007/s00190-007-0148-y.
- Steigenberger, P., V. Tesmer, M. Krügel, D. Thaller, R. Schmid, S. Vey, and M. Rothacher (2007), Comparison of homogeneously reprocessed GPS and VLBI long time-series of troposphere zenith wet delays and gradients, *J. Geod.*, *81*, 503–514, doi:10.1007/s00190-006-0124-y.
- Stowell, B., T. Nilsson, G. Elgered, and P. O. J. Jarlemark (2007), Temporal correlations of atmospheric mapping function errors in GPS estimation, *J. Geod.*, *81*(5), 311–323, doi:10.1007/s00190-006-0114-0.
- Tralli, D. M., and S. M. Lichten (1990), Stochastic estimation of tropospheric path delays in Global Positioning System geodetic measurements, *Bull. Geod.*, *64*, 127–159.
- Trenberth, K. E., A. Dai, R. Rasmussen, and D. Parsons (2003), The changing character of precipitation, *Bull. Am. Meteorol. Soc.*, *84*(9), 1205–1217, doi:10.1175/BAMS-84-9-1205.
- Trenberth, K. E., J. Fasullo, and L. Smith (2005), Trends and variability in column-integrated water vapor, *Clim. Dyn.*, *24*, 741–758, doi:10.1007/s00382-005-0017-4.
- Wang, J., L. Zhang, and A. Dai (2005), Global estimates of water-vapor-weighted mean temperature of the atmosphere for GPS applications, *J. Geophys. Res.*, *110*, D21101, doi:10.1029/2005JD006215.
- Wessel, P., and W. H. F. Smith (1998), New, improved version of generic mapping tools released, *Eos Trans. AGU*, *79*(47), 579.

G. Elgered and T. Nilsson, Onsala Space Observatory, Department of Radio and Space Science, Chalmers University of Technology, SE 43992 Onsala, Sweden. (tobias.nilsson@chalmers.se)